We are IntechOpen, the world's leading publisher of Open Access books Built by scientists, for scientists

4,800
Open access books available

122,000
International authors and editors

135M
Downloads

Our authors are among the

154
Countries delivered to

TOP 1%
most cited scientists

12.2%
Contributors from top 500 universities

CLARIVATE ANALYTICS BOOK CITATION INDEX INDEXED

WEB OF SCIENCE™

Selection of our books indexed in the Book Citation Index in Web of Science™ Core Collection (BKCI)

Interested in publishing with us?
Contact book.department@intechopen.com

Numbers displayed above are based on latest data collected.
For more information visit www.intechopen.com

21

Electromechanical Fields in Quantum Heterostructures and Superlattices

Lars Duggen and Morten Willatzen
Mads Clausen Institute, University of Southern Denmark
Denmark

1. Introduction

The study of quantum semiconductor structures has received much attention in recent years. Especially group III nitrides have been of considerable interest due to their potential applications as LEDs and laser diodes in the UV region (Kneissl et al., 2003; Nakamura et al., 1994; Yoshida et al., 2008a;b). But also other materials, as the group II oxides have been investigated for their potential as highly efficient laser diodes (Fan et al., 2006; Fujita et al., 2004). Typically, these materials are in the wurtzite crystal phase. Nevertheless some of these materials also exist in the zincblende crystal phase. Furthermore there are the more classical materials as AlGaAs that are in zincblende phase. For this reason we chose to focus on these two crystal structures throughout this chapter.

As opposed to other semiconductor materials as silicone, the above mentioned materials generate electric fields when deformed and vice versa. This so called piezoelectric effect plays a significant role for both band structure and optical gain (Park & Chuang, 1998), which is why it is important to investigate.

In this chapter we start by covering the properties of the wurtzite and zincblende crystal structures and proceed by presenting definitions of stress and strain followed by a derivation of the constitutive relations for the piezoelectric effect from thermodynamic considerations. After establishing the governing equations and justifying for the electrostatic approximation we apply these to a single quantum well structure. Then we present the according calculations for a cylindrical quantum dot along with results from current research papers. We give a brief discussion about the validity of these models and possibilities for improving these. To give a better overview, we briefly present the VFF model as an alternative method for determining strains in quantum wells.

Finally we give a simplified mathematical description of the connection between the computed electromechanical fields and the optical and electrical properties of the quantum structures. Also we provide tables containing various material parameters needed to compute the electromechanical fields as described in this chapter.

2. Crystal structures

As mentioned, there are two predominant crystal structures in semiconductor technology that have piezoelectric properties: zincblende and wurtzite. Silicon based semiconductors are not piezoelectric and will not be covered in this chapter.

A sketch of the zincblende unit cell is shown in Figure 1. zincblende is a combination of two face-centered cubic (fcc) crystals, where one of them is offsetted by $a/4, a/4, a/4$, a being the lattice constant which in this case is the length the cubic edges. It looks quite similar to the diamond structure, but as opposed to the latter, the zincblende structure consists of ionic bonds, causing a nonhomogeneous charge distribution. Macroscopically however, all dipole moments cancel each other and the nonhomogeneous charge distribution is not visible as long as it is not deformed. Notable semiconductor materials that can be fabricated in zincblende form are arsenides such as GaAs, AlAs, or InAs; nitrides such as GaN, AlN, InN, as well as oxides such as ZnO (Auld, 1990; Davydov, 2002; Fonoberov & Balandin, 2003; J.I.Izpura et al., 1999; Vurgaftman et al., 2001).

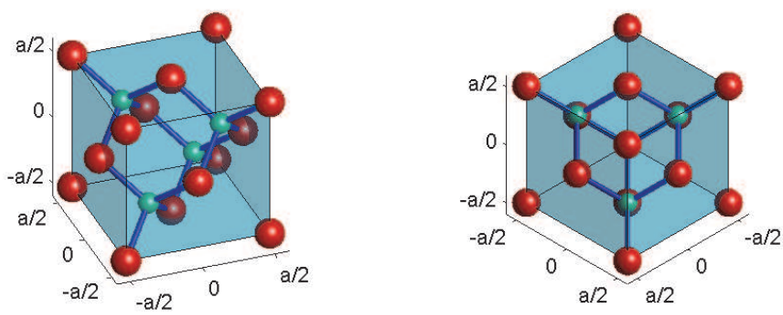

Fig. 1. The zincblende unit cell observed from two different angles. The colors represent the respective atom as e.g. Ga and As for GaAs. Due to ionic bonding they possess different charges. Note that the unit cell to the right has an appearance resembling a hexagonal structure. Indeed we will show that this crystal orientation exhibits piezoelectric properties resembling those of wurtzite (albeit there still are differences)

The other important crystal structure is wurtzite, which is sketched in Figures 2-3. Wurtzite is a hexagonal crystal and, opposed to zincblende, possesses spontaneous polarization, a built-in net polarization in the c-axis direction. Important semiconductor materials grown in wurtzite form include nitrides such as GaN, AlN, and InN as well as oxides such as ZnO and MgO (Fonoberov & Balandin, 2003; Gopal & Spaldin, 2006; Vurgaftman et al., 2001).

2.1 Miller indices

As we will cover the effect of crystal orientation in this chapter, we will briefly introduce the use of Miller indices. They are written in square brackets and consist of three integer digits, i.e. the form is [klm]. The integers refer to directions with respect to the crystal basis. For cubic crystal classes as zincblende the basis vectors are simply the three orthogonal vectors coinciding with the cube edges as can be seen in Figure 4. Note that the indices also describe the orientation of crystal planes by denoting their normal vector. This can be used to construct the indices since one can use intersection points with the basis vectors and invert them. For example a crystal plane with the direction $[112]$ intersects the basis at points $[1,0,0]$, $[0,1,0]$, and $[0,0,1/2]$. This crystal plane then gives the cross section one would see when looking at a crystal in this direction. When denoting a plane directly then one typically uses parenthesis instead of square brackets. Negative directions are denoted by a bar over the respective index. For example $[\bar{k}\bar{k}\bar{k}]$ is exactly the opposite of $[kkk]$. For hexagonal classes such as wurtzite, the basis vectors are shown in Figure 4. It should be mentioned however, that in crystallography

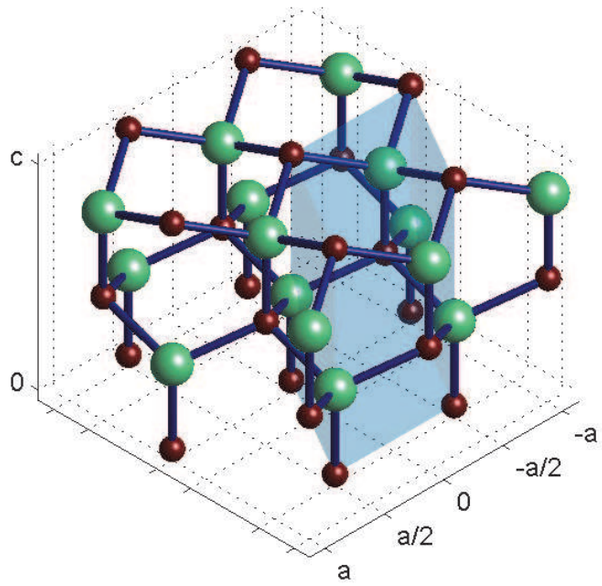

Fig. 2. The wurtzite crystal structure. For clearer impression of the hexagonal symmetry, more than one unit cell is drawn. One unit cell is indicated by the transparent blue box. Also here the atomic bonds are predominantly of ionic nature.

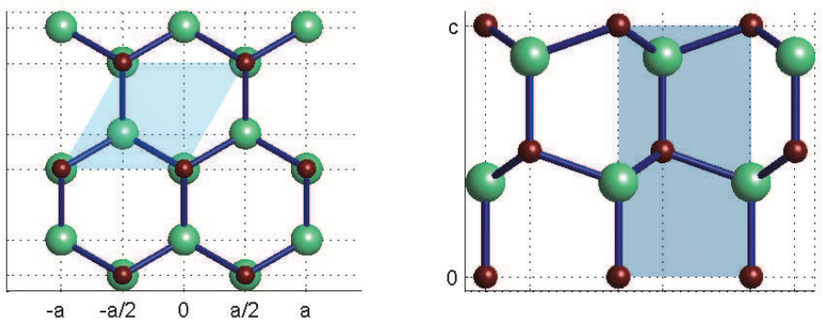

Fig. 3. Top view of the wurtzite structure (left). Here the hexagonal symmetry becomes clear. Side view of the wurtzite structure (right). Note the lack of inversion symmetry which causes both piezoelectric behavior and spontaneous polarization

it is quite common to denote directions in hexagonal crystals by four indices, of which one is redundant. These so called Bravais-Miller indices can be constructed from the standard Miller indices by $[klm] \rightarrow [kl-(h+k)m]$.

3. Fundamental equations

As we are dealing with electromechanical fields, we need fundamental equations for both the mechanical and the electrical part as well as equations for coupling these. In this section we will cover the definitions of linear stress and strain and develop a linear description of the

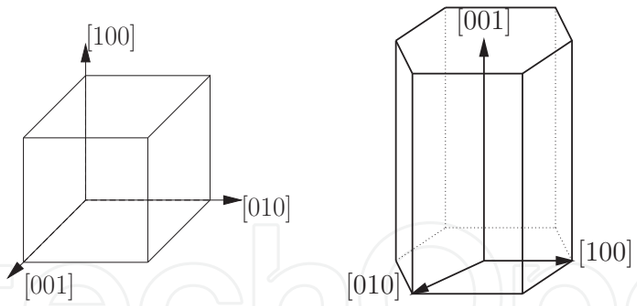

Fig. 4. Basis vectors of the cubic crystal (left) and the hexagonal crystal (right)

piezoelectric effect. Furthermore we will present Maxwell's equations in differential form and derive Navier's law as a linearized form of Newton's Second law. Note that we will stay entirely within the domain of classical physics.

3.1 Stress, strain, and the Piezoelectric effect

The need of a precise definition of deformation of a material should be rather obvious. He we consider material as a continuum consisting of infinitely many, infinitely small elements. Let $\mathbf{r}$ be the position of such an element. Then let $\mathbf{u}$ be the dislocation of the element, i.e. $\mathbf{u} = \mathbf{r} - \mathbf{r_0}$. In general, $\mathbf{u}$ is a function of both space and time, but it does not give a measure of deformation, since it can be non-zero also for undeformed shapes. As an example, taking the gradient of $\mathbf{u}$ will prove insufficient as well, since rotation of an undeformed shape will be non-zero (Landau & Lifshitz, 1986). However, introducing the strain as (Auld, 1990; Landau & Lifshitz, 1986)

$$S_{ij} = \frac{1}{2}\left(\frac{\partial u_i}{\partial r_j} + \frac{\partial u_j}{\partial r_i} + \frac{\partial u_k}{\partial r_i}\frac{\partial u_k}{\partial r_j}\right), \tag{1}$$

allows us to obtain zero if and only if the shape in question is deformed. Assuming that we only work with small $\mathbf{u}$ quantities we can neglect the second order terms to arrive at the definition of linear strain

$$S_{ij} = \frac{1}{2}\left(\frac{\partial u_i}{\partial r_j} + \frac{\partial u_j}{\partial r_i}\right). \tag{2}$$

As we deform a shape of a certain material, obviously we do also create restoring forces. Defining these forces we consider an infinitely small volume element $\delta V = \delta x \delta y \delta z$. Then we can consider traction forces one each of the sides of the element (x, y, and z sides), that is three force vectors:

$$\begin{aligned} \mathbf{T}_x &= T_{xx}\hat{\mathbf{x}} + T_{xy}\hat{\mathbf{y}} + T_{xz}\hat{\mathbf{z}}, \\ \mathbf{T}_y &= T_{yx}\hat{\mathbf{x}} + T_{yy}\hat{\mathbf{y}} + T_{yz}\hat{\mathbf{z}}, \\ \mathbf{T}_z &= T_{zx}\hat{\mathbf{x}} + T_{zy}\hat{\mathbf{y}} + T_{zz}\hat{\mathbf{z}}. \end{aligned} \tag{3}$$

The second order tensor consisting of the entries T_{ij} is called the stress tensor and is a measure of pressure.

As long as we stay within the elastic limit, the shape will be restored to its original state once all deformation forces are removed. In other words, the process is reversible and we can treat it thermodynamically. The fundamental thermodynamic relation for deformed bodies reads(Landau & Lifshitz, 1986)

$$dU_{\text{mech}} = \Theta d\sigma + T_{ik} dS_{ik}, \tag{4}$$

where dU_{mech} is the change in internal energy, Θ is the temperature, σ is the entropy, and summation over indices is implicit. However, we have seen that deformations in a piezoelectric material give rise to an electric polarization, stipulating that one needs to take electrical energy into account as well. This contribution reads (Landau et al., 1984)

$$dU_{\text{elec}} = E_i dD_i, \tag{5}$$

where E_i and D_i denote the ith electric and displacement field component, respectively. Conclusively the total change in internal energy is

$$dU = \Theta d\sigma + T_{ik} dS_{ik} + E_i dD_i. \tag{6}$$

It will prove convenient however, to look at other thermodynamic quantities as well. Here we chose the electric enthalpy H_{elec}, as this will yield the equation we will use later on. For other interesting quantities and a more detailed derivation of these, see Willatzen (2001). Defining

$$H_{\text{elec}} = U - E_i D_i, \tag{7}$$

we obtain the differential

$$\begin{aligned} dH_{\text{elec}} &= dU - d(E_i D_i) \\ &= dU - E_i dD_i - D_i dE_i \\ &= \Theta d\sigma - D_i dE_i + T_{kl} dS_{kl}. \end{aligned} \tag{8}$$

Furthermore it is common to assume isentropic operation (Auld, 1990; Willatzen, 2001), even though in principle isothermal operation is possible as well. However, isothermal operation is hard to achieve due to energy dissipation and it has been found experimentally that the isentropic assumption works quaite well (Auld, 1990). In the following we will always assume constant entropy without denoting it specifically.
We will chose to use the thermodynamic state variables **E** and **S**. Then we express the two remaining variables **D** and **T** as

$$D_i = \left(\frac{\partial D_i}{\partial E_j}\right)_S E_j + \left(\frac{\partial D_i}{\partial S_{kl}}\right)_E S_{kl}, \tag{9}$$

$$T_{kl} = \left(\frac{\partial T_{kl}}{\partial E_j}\right)_S E_j + \left(\frac{\partial T_{kl}}{\partial S_{mn}}\right)_E S_{mn}, \tag{10}$$

where the subscript at the partial derivatives denotes the field that is held constant. Furthermore we have used the zero-reference to arrive at these equations.

Notice that we can describe the above derivatives as derivatives of H_{elec} and define a constant, such that (using that order of differentiation is arbitrary)

$$e_{ikl} \equiv \left(\frac{\partial D_i}{\partial S_{kl}}\right)_E = -\left(\frac{\partial^2 H_{\text{elec}}}{\partial S_{kl}\partial E_i}\right) = -\left(\frac{\partial^2 H_{\text{elec}}}{\partial E_i \partial S_{kl}}\right)$$
$$= -\left(\frac{\partial T_{kl}}{\partial E_i}\right)_S = e_{kli}, \tag{11}$$

$$c^E_{klmn} = \left(\frac{\partial T_{kl}}{\partial S_{mn}}\right)_E, \qquad \epsilon^S_{ij} = \left(\frac{\partial D_i}{\partial E_j}\right)_S \tag{12}$$

Note the transposition symmetry $e_{ikl} = e_{kli}$. Similarly it can be shown that $c^E_{klmn} = c^E_{mnkl}$ and $\epsilon^S_{ij} = \epsilon^S_{ji}$. Regarding these constants as material constants we can rewrite the piezoelectric equations as

$$D_i = \epsilon^S_{ij} E_j + e_{ikl} S_{kl} + P^{sp}_i, \tag{13}$$

$$T_{kl} = -e_{kli} E_i + c^E_{klmn} S_{mn}, \tag{14}$$

where the first equation is the direct effect while the latter is called the converse effect. The vector $\mathbf{P}^{sp}$ denotes spontaneous polarization, which is zero for zincblende crystals and has a nonzero z-component for wurtzite. It should be mentioned already here that there are generally two common approaches to these equations when dealing with quantum structures. One is the fully-coupled approach, where the equations above are used as they are, while the other approach is the semi-coupled one where the piezoelectric tensor **e** for the converse effect is neglected.

3.1.1 Voigt notation

Due to the symmetry of the tensors involved in the piezoelectric fundamental equations it is possible and useful to contract the index notation. This will transform the nine-element strain and stress tensors to six-element vectors. The subscript contraction for Cartesian coordinates is as follows:

$$xx \to 1, yy \to 2, zz \to 3, \tag{15}$$

$$yz \;\&\; zy \to 4, xz \;\&\; zx \to 5, xy \;\&\; yx \to 6. \tag{16}$$

Note that the piezoelectric stiffness tensor e cannot be fully reduced since it is of third rank. Thus one reduces only the kl-set from equations (13) and (14) such that one can use standard matrix multiplication rules once contracted.

It should also be mentioned that there exist different standards with respect to weights when contraction. One standard is to use the same weight (typically 1) for both stress and strain. Another standard, used by Auld (1990), is to multiply the three shear strains by two while using unit weight for the stress, i.e

$$S_I = 2 \cdot S_{ij} - \delta_{ij} S_{ij}, \qquad i,j = 1,2,3, I = 1,2,3,4,5,6, \tag{17}$$

$$T_I = T_{ij} \qquad i,j = 1,2,3, I = 1,2,3,4,5,6. \tag{18}$$

We will use the latter standard as the resulting contraction operations for the stiffnesses are weightless and thus can be taken directly from several sources containing many of these constants, such as Vurgaftman et al. (2001).

$$c_{IJ} = c_{klmn},\ e_{iK} = e_{ikl}. \tag{19}$$

Tensors that already are of second rank are not contracted. Using this contraction, the piezoelectric relations read

$$\mathbf{D} = \varepsilon^S \mathbf{E} + \mathbf{eS} + \mathbf{P}^{sp}, \tag{20}$$

$$\mathbf{T} = -\mathbf{e}^T \mathbf{E} + \mathbf{c}^E \mathbf{S}, \tag{21}$$

where ε is the 3×3 permittivity matrix, $\mathbf{e}$ is the 3×6 piezoelectric matrix, $\mathbf{c}$ is the 6×6 stiffness, while $\mathbf{D}, \mathbf{E}$ are the 3×1 electric displacement and electric field vectors, respectively, and $\mathbf{T}, \mathbf{S}$ are the 6×1 stress and strain vectors, respectively.

3.2 Material property tensors

For the sake of completeness we give the general form of the material properties of wurtzite and zincblende.

3.2.1 Wurtzite

The wurtzite crystal structure has three independent entries in the piezoelectric tensor, four in the stiffness tensor and two in the purely diagonal permittivity tensor. The matrices read

$$\begin{aligned}
\mathbf{e} &= \begin{bmatrix} 0 & 0 & 0 & 0 & e_{x5} & 0 \\ 0 & 0 & 0 & e_{x5} & 0 & 0 \\ e_{z1} & e_{z1} & e_{z3} & 0 & 0 & 0 \end{bmatrix}, \\
\mathbf{c} &= \begin{bmatrix} c_{11} & c_{12} & c_{13} & 0 & 0 & 0 \\ c_{12} & c_{11} & c_{13} & 0 & 0 & 0 \\ c_{13} & c_{13} & c_{33} & 0 & 0 & 0 \\ 0 & 0 & 0 & c_{44} & 0 & 0 \\ 0 & 0 & 0 & 0 & c_{44} & 0 \\ 0 & 0 & 0 & 0 & 0 & \frac{1}{2}(c_{11} - c_{12}) \end{bmatrix}, \\
\varepsilon &= \begin{bmatrix} \epsilon_{xx} & 0 & 0 \\ 0 & \epsilon_{xx} & 0 \\ 0 & 0 & \epsilon_{zz} \end{bmatrix}, \\
\mathbf{P}^{SP} &= \begin{bmatrix} 0 \\ 0 \\ p^{SP} \end{bmatrix}
\end{aligned} \tag{22}$$

3.2.2 Zincblende

For zincblende there is only one independent entry for the piezoelectric coupling e_{x4} and three independent entries for the stiffness tensor $\mathbf{c}$ while the permittivity in fact can be used as a scalar ϵ_{xx} since all the diagonal entries in the purely diagonal matrix are the same. The

matrices read

$$\mathbf{e} = \begin{bmatrix} 0 & 0 & 0 & e_{x4} & 0 & 0 \\ 0 & 0 & 0 & 0 & e_{x4} & 0 \\ 0 & 0 & 0 & 0 & 0 & e_{x4} \end{bmatrix},$$

$$\mathbf{c} = \begin{bmatrix} c_{11} & c_{12} & c_{12} & 0 & 0 & 0 \\ c_{12} & c_{11} & c_{12} & 0 & 0 & 0 \\ c_{12} & c_{12} & c_{11} & 0 & 0 & 0 \\ 0 & 0 & 0 & c_{44} & 0 & 0 \\ 0 & 0 & 0 & 0 & c_{44} & 0 \\ 0 & 0 & 0 & 0 & 0 & c_{44} \end{bmatrix},$$

$$\varepsilon = \begin{bmatrix} \epsilon_{xx} & 0 & 0 \\ 0 & \epsilon_{xx} & 0 \\ 0 & 0 & \epsilon_{xx}. \end{bmatrix} \tag{23}$$

3.3 Higher order electromechanical effects

This chapter will not cover the handling of nonlinear electromechanical effects. Nevertheless the importance of these effects is being discussed in literature (Voon & Willatzen, 2011) and for this reason we will give a brief introduction to second order piezoelectricity. The other effect, electrostriction, should also be mentioned here. It is a second order effect between strain and the electric field, with the governing equation reading (Newnham et al., 1997)

$$S_{ij} = M_{ijkl} E_k E_l. \tag{24}$$

Note that, opposed to the piezoelectric effect, M_{ijkl} is a tensor of even rank and thus this effect does not need breaking of symmetry as the piezoelectric effect does. However, it is very difficult to estimate the impact of this effect since the electrostrictive tensor is very hard to measure correctly (Voon & Willatzen, 2011).

3.3.1 Second order Piezoelectricity

Instead of assuming a linear relationship between the piezoelectrically generated field and the strain, it is also possible to assume relationships of second order. This yields a piezoelectric tensor that does depend on the strain itself and reads (Bester, Wu, Vanderbilt & Zunger, 2006; Bester, Zunger, Wu & Vanderbilt, 2006)

$$e_{iJ} = e^0_{iJ} + \sum_{k=1}^{6} B_{iJK} S_K, \tag{25}$$

where e^0_{iJ} is the piezoelectric tensor at zero strain and B_{iJK} is the fifth rank tensor representing the non-linear piezoelectric effect. Theoretically, the impact of this effect has been shown to be of significance (Bester, Wu, Vanderbilt & Zunger, 2006; Bester, Zunger, Wu & Vanderbilt, 2006), however the agreement with experiments is still disputed (see also discussion in Voon & Willatzen (2011)).

3.4 Navier's and Maxwell's equations

As we deal with coupled electrical and mechanical effects we will need the field equations for both. The electromagnetic field equations consist of the four Maxwell equations

$$\nabla \times \mathbf{E} = -\frac{\partial \mathbf{B}}{\partial t}, \tag{26}$$

$$\nabla \times \mathbf{H} = \frac{\partial \mathbf{D}}{\partial t} + \mathbf{J}_c + \mathbf{J}_s, \tag{27}$$

$$\nabla \cdot \mathbf{B} = 0, \tag{28}$$

$$\nabla \cdot \mathbf{D} = \rho_e, \tag{29}$$

where we have chosen the differential form and $\mathbf{H}$ denotes the magnetic field intensity, $\mathbf{B}$ denotes the magnetic flux density and $\mathbf{J}_c, \mathbf{J}_s$ denote conduction and source currents, respectively, while ρ_e is the free electric charge density. For further details on the origin of these equations the reader is referred to Landau & Lifshitz (1975).

The mechanical field equation of course has its origin in Newton's Second law. Considering a small volume δV with surface δS we have the balance of forces

$$\int_{\delta S} \mathbf{T}\hat{\mathbf{n}}\, dS + \int_{\delta V} \mathbf{F}\, dV = \int_{\delta V} \rho_m \frac{\partial^2 \mathbf{u}}{\partial t^2} dV, \tag{30}$$

where the first integral is the summation of surface forces, the second is due to the possible presence of a body force $\mathbf{F}\delta V$ and ρ_m is the mass density. In the case where $\delta V \to 0$ the integrands can be regarded as being constant and we obtain Navier's equation

$$\nabla \cdot \mathbf{T} = \rho_m \frac{\partial^2 \mathbf{u}}{\partial t^2} - \mathbf{F}, \tag{31}$$

where $\nabla \cdot \mathbf{T} \equiv \lim_{\delta V \to 0} \frac{\int_{\delta S} \mathbf{T}\hat{\mathbf{n}}\, dS}{\delta V}$. In Cartesian coordinates the divergence of stress $\nabla \cdot \mathbf{T}$ reads

$$(\nabla \cdot \mathbf{T})_i = \frac{\partial T_{ij}}{\partial r_j}, \tag{32}$$

where $i, j = x, y, z$. In Voigt notation, the divergence can be expressed by a 3×6 matrix which in Cartesian coordinates reads

$$\nabla \cdot \to \begin{bmatrix} \frac{\partial}{\partial x} & 0 & 0 & 0 & \frac{\partial}{\partial z} & \frac{\partial}{\partial y} \\ 0 & \frac{\partial}{\partial y} & 0 & \frac{\partial}{\partial z} & 0 & \frac{\partial}{\partial x} \\ 0 & 0 & \frac{\partial}{\partial z} & \frac{\partial}{\partial y} & \frac{\partial}{\partial x} & 0 \end{bmatrix} \tag{33}$$

Forms for other coordinate systems can be obtained by considering an elementary volume of this coordinate system and making a linear approximation of the stresses $\mathbf{T}$ on the surfaces on that volume, finally letting the volume approach zero. The divergence for cylindrical and spherical systems are also given in Auld (1990).

With Maxwell's and Navier's equations together with the piezoelectric constitutive relations we have the complete basis for computing electrical and mechanical fields in piezoelectric materials (neglecting second order terms as electrostriction).

3.4.1 Electrostatic approximation

When dealing with problems that are constant in time, the electromagnetic coupling is non-existent and the only equations left to solve are Navier's equation along with the following two of Maxwell's equations

$$\nabla \times \mathbf{E} = 0,\ \nabla \cdot \mathbf{D} = \rho_e. \tag{34}$$

With time varying problems on the other hand, one needs to solve all of Maxwell's and Navier's equations self-consistently. However, in most cases (Auld, 1990) it is possible to use the electrostatic approximation, forcing $\nabla \times \mathbf{E} = 0$ and introducing an insignificant error. Here we will justify this on a simple example and leave further discussions to Auld (1990).

Consider an electromechanical plane wave in the z-direction of a bulk piezoelectric material with zero free electric charges of general crystal structure (however, for simplicity considering diagonal terms in ε only as well as assuming non-magnetic properties, as is always the case for either wurtzite or zincblende). In this case we will not be able to assume that also $\mathbf{B}$ and $\mathbf{H}$ depend on z only. After some manipulation using Maxwell's and Navier's equations, one arrives at the dispersion relation

$$\begin{bmatrix} \Gamma_{53}\frac{k^2}{\omega^2} & \Gamma_{54}\frac{k^2}{\omega^2} & \Gamma_{55}\frac{k^2}{\omega^2} - \rho_m & -e_{5x}\frac{k^2}{\omega^2} & -e_{5y}\frac{k^2}{\omega^2} \\ \Gamma_{43}\frac{k^2}{\omega^2} & \Gamma_{44}\frac{k^2}{\omega^2} - \rho_m & \Gamma_{45}\frac{k^2}{\omega^2} & -e_{4x}\frac{k^2}{\omega^2} & -e_{4y}\frac{k^2}{\omega^2} \\ \Gamma_{33}\frac{k^2}{\omega^2} - \rho_m & \Gamma_{34}\frac{k^2}{\omega^2} & \Gamma_{35}\frac{k^2}{\omega^2} & -e_{3x}\frac{k^2}{\omega^2} & -e_{3y}\frac{k^2}{\omega^2} \\ \mu_0 e_{x3} & \mu_0 e_{x4} & \mu_0 e_{x5} & \mu_0\epsilon_{xx} - \frac{k^2}{\omega^2} & 0 \\ \mu_0 e_{y3} & \mu_0 e_{y4} & \mu_0 e_{y5} & 0 & \mu_0\epsilon_{yy} - \frac{k^2}{\omega^2} \end{bmatrix} \cdot \begin{bmatrix} S_3 \\ S_4 \\ S_5 \\ E_x \\ E_y \end{bmatrix} = \mathbf{0}, \tag{35}$$

where Γ denotes the piezoelectrically stiffened elastic tensor given by

$$\Gamma = \mathbf{c}^E + \frac{\mathbf{e}^T\mathbf{e}}{\epsilon}^{-1}. \tag{36}$$

Considering standard numerical values of the material properties, i.e. $\Gamma \sim 10^{10}, \rho_m \sim 10^3, e_{iJ} \sim 1, \epsilon \sim 10^{-11}, \mu_0 = 4\pi \cdot 10^{-7}$ it is easily seen that there is only a weak coupling between the submatrices $1-3 \times 1-3$ and $4-5 \times 4x5$. When computing the determinant of this matrix as the sum of all permutation products (negating sign for odd permutations) it becomes clear that the elements with three Γ contributions are dominating in the range of $k^2/\omega^2 = 1/c^2$ with $c \sim 10^3$. The summation terms including three Γ contributions are of order 10^0 while the terms including only two Γ contributions are of order 10^{-6}.

On the other hand, for large ω so we are getting close to electromagnetic wave propagation, we have $c \sim 10^8$. Then the one dominating term becomes $\sim -\rho_m^3\mu_0\epsilon_{xx}\mu_0\epsilon_{yy} \sim 10^{-25}$, with the second largest terms $\sim 10^{-34}$.

Note that in the absence of piezoelectricity we obtain the uncoupled dispersion relations for acoustic and electromagnetic wave propagation, respectively. Thus the piezoelectric coupling terms in the dispersion relation are negligible and one obtains the same dispersion relation as with the electrostatic approximation, where only the $1-3 \times 1-3$ submatrix will occur in the dispersion and the electromagnetic wave is considered to be purely electromagnetic. Even more, the amplitudes of the strain elements and the electric field elements will also only be perturbed insignificantly.

4. Quantum structures

The key issue for investigating piezoelectric effects in the wurtzite and zincblende crystal structures is their widespread use in optoelectronics and electronics in general. Here we will focus on "clean" quantum structures, i.e. without doping. The major reason for the use of materials such as GaN, AlN and others is their large electronic band gap creating the possibility of large energy transitions as necessary for UV-leds. A basic sketch of a quantum well structure is shown in Figure5

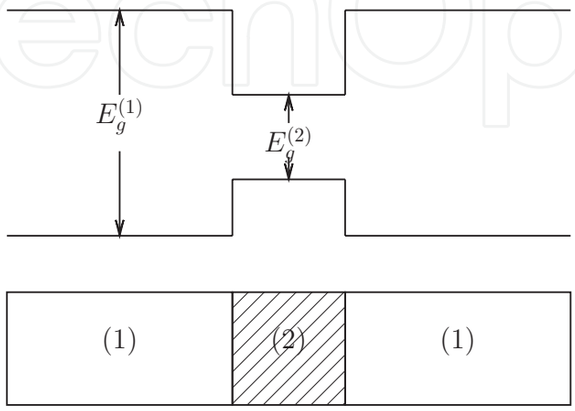

Fig. 5. Basic sketch of a quantum well structure. The indices (1) and (2) denote barrier and well material, respectively. The upper part indicates the conduction and valence band energies for zero electric field.

The three types of quantum structures that differ in the number of confined dimensions are

- Quantum well: one dimension confined
- Quantum wire: two dimensions confined
- Quantum dot: three dimensions confined

One motivation for investigation of these types is that a decrease of dimensionality is reflected in the density of state functions of these structures. The dependency of the density of states (DOS), denoted $N(E)$, on the energy E functions read in a one-band effective model (Singh, 2003)

$$N(E)_{\text{bulk}} = \frac{\sqrt{2}m^{*3/2}\sqrt{E-E_c}}{\pi^2\hbar^3}, \tag{37}$$

$$N(E)_{\text{well}} = \frac{m^*}{\pi\hbar^2};\ E > E_i(\text{from each subband } i), \tag{38}$$

$$N(E)_{\text{wire}} = \frac{\sqrt{2}m^{*1/2}}{\pi\hbar}(E-E_i)^{-1/2};\ E > E_i(\text{from each subband } i), \tag{39}$$

$$N(E)_{\text{dot}} = \delta(E-E_i), \tag{40}$$

where E_c is the conduction band energy and m^* is the electron effective mass. Note that the DOS for a quantum dot is discrete, i.e. a quantum dot is treated as a single, isolated particle. A thorough discussion about these three structures can be found in Singh (2003).
The theory presented in this chapter covers electromechanical fields of both well and barrier structures, the latter being used for transistor technology (Koike et al., 2005; Sasa et al., 2006).

5. One-dimensional electromechanical fields in quantum wells

This section contains an example for the application of the above equations on quantum wells. For simplicity we will assume no free charges in the structure as this removes the necessity of solving the Schrödinger equation simultaneously.
The well layer (2) will adapt its lattice constant to the barriers (1) and the strain in the well layer is defined as (Ipatova et al., 1993)

$$\mathbf{S}^{(2)} = \begin{bmatrix} \frac{\partial u_x^{(2)}}{\partial x} - a_{mis} \\ \frac{\partial u_y^{(2)}}{\partial y} - a_{mis} \\ \frac{\partial u_z^{(2)}}{\partial z} - c_{mis} \\ \frac{\partial u_y^{(2)}}{\partial z} + \frac{\partial u_z^{(2)}}{\partial y} \\ \frac{\partial u_x^{(2)}}{\partial z} + \frac{\partial u_z^{(2)}}{\partial x} \\ \frac{\partial u_x^{(2)}}{\partial y} + \frac{\partial u_y^{(2)}}{\partial x} \end{bmatrix}, \tag{41}$$

while the strain in layer (1) is defined as usual (see equation (1)). This definition is for wurtzite structures, having two lattice constants a, c. The mismatch a_{mis} is given by $a_{mis} = \left(a^{(2)} - a^{(1)}\right)/a^{(1)}$ and c_{mis} is defined similarly. For use with zincblende, $c_{mis} = a_{mis}$. For the quantum well it is often assumed that all quantities depend exclusively on the z-direction and the x, y-directions are infinite. Note that, since we are working with first order strain, the choice of the denominator for a_{mis} and c_{mis} is arbitrary, as the difference $\left(a^{(2)} - a^{(1)}\right)/a^{(1)} - \left(a^{(2)} - a^{(1)}\right)/a^{(2)}$ is of second order.

5.1 Crystal orientation

As already discussed, the zincblende structure does not exhibit piezoelectric properties upon hydrostatic compression (i.e. no shear). However, as seen in Figure 1 there is reason to believe that a rotation of the crystal structure yields a piezoelectric field upon hydrostatic compression.
The rotation of unit cells is modeled by a rotation of the describing coordinate system transforming coordinates $x, y, z \rightarrow x', y', z'$. The transformation is performed by two subsequent rotations around coordinate axis as shown in Figure 6. The different quantities then transform as

$$\mathbf{r}' = \mathbf{a} \cdot \mathbf{r}, \qquad \mathbf{P}^{SP'} = \mathbf{a} \cdot \mathbf{P}^{SP},$$
$$\mathbf{T}' = \mathbf{M} \cdot \mathbf{T}, \qquad \mathbf{S}' = \mathbf{N} \cdot \mathbf{S},$$
$$\mathbf{E}' = \mathbf{a} \cdot \mathbf{E}, \qquad \mathbf{D}' = \mathbf{a} \cdot \mathbf{D},$$
$$\varepsilon' = \mathbf{a} \cdot \varepsilon \cdot \mathbf{a}^T, \qquad \mathbf{e}' = \mathbf{a} \cdot \mathbf{e} \cdot \mathbf{M}^T,$$
$$\mathbf{c}^{\mathbf{E}'} = \mathbf{M} \cdot \mathbf{c}^{\mathbf{E}} \cdot \mathbf{M}^T,$$

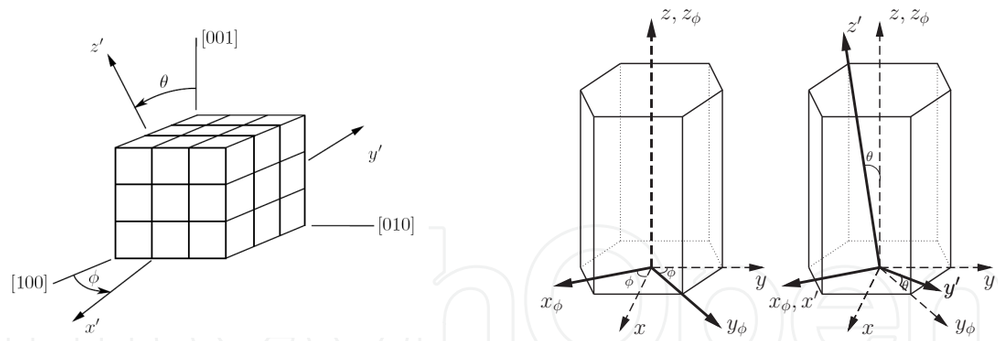

Fig. 6. Subsequent coordinate system rotations - ϕ around z followed by θ around the new x-axis. The cubes to the left indicate the cubic crystal structure while the middle and right figures represent the same operation for hexagonal crystals. Reprinted with permission from Duggen et al. (2008) and Duggen & Willatzen (2010).

where $\mathbf{a}$ is given by (Auld, 1990; Goldstein, 1980)

$$\mathbf{a} = \begin{bmatrix} \cos(\phi) & \sin(\phi) & 0 \\ -\cos(\theta)\sin(\phi) & \cos(\theta)\cos(\phi) & \sin(\theta) \\ \sin(\theta)\sin(\phi) & -\sin(\theta)\cos(\phi) & \cos(\theta) \end{bmatrix}, \tag{42}$$

and the $\mathbf{M}, \mathbf{N}$ matrices are called Bond stress and strain transformation matrices, respectively. They are constructed out of the elements of $\mathbf{a}$ as given in the following (Auld, 1990; Bond, 1943):

$$\mathbf{M} = \begin{bmatrix} a_{11}^2 & a_{12}^2 & a_{13}^2 & 2a_{12}a_{13} & 2a_{13}a_{11} & 2a_{11}a_{12} \\ a_{21}^2 & a_{22}^2 & a_{23}^2 & 2a_{22}a_{23} & 2a_{23}a_{21} & 2a_{21}a_{22} \\ a_{31}^2 & a_{32}^2 & a_{33}^2 & 2a_{32}a_{33} & 2a_{33}a_{31} & 2a_{31}a_{32} \\ a_{21}a_{31} & a_{22}a_{32} & a_{23}a_{33} & a_{22}a_{33}+a_{23}a_{32} & a_{21}a_{33}+a_{23}a_{31} & a_{22}a_{31}+a_{21}a_{32} \\ a_{31}a_{11} & a_{32}a_{12} & a_{33}a_{13} & a_{12}a_{33}+a_{13}a_{32} & a_{13}a_{31}+a_{11}a_{33} & a_{11}a_{32}+a_{12}a_{31} \\ a_{11}a_{21} & a_{12}a_{22} & a_{13}a_{23} & a_{12}a_{23}+a_{13}a_{22} & a_{13}a_{21}+a_{11}a_{23} & a_{11}a_{22}+a_{12}a_{21} \end{bmatrix}, \tag{43}$$

$$\mathbf{N} = \begin{bmatrix} a_{11}^2 & a_{12}^2 & a_{13}^2 & a_{12}a_{13} & a_{13}a_{11} & a_{11}a_{12} \\ a_{21}^2 & a_{22}^2 & a_{23}^2 & a_{22}a_{23} & a_{23}a_{21} & a_{21}a_{22} \\ a_{31}^2 & a_{32}^2 & a_{33}^2 & a_{32}a_{33} & a_{33}a_{31} & a_{31}a_{32} \\ 2a_{21}a_{31} & 2a_{22}a_{32} & 2a_{23}a_{33} & a_{22}a_{33}+a_{23}a_{32} & a_{21}a_{33}+a_{23}a_{31} & a_{22}a_{31}+a_{21}a_{32} \\ 2a_{31}a_{11} & 2a_{32}a_{12} & 2a_{33}a_{13} & a_{12}a_{33}+a_{13}a_{32} & a_{13}a_{31}+a_{11}a_{33} & a_{11}a_{32}+a_{12}a_{31} \\ 2a_{11}a_{21} & 2a_{12}a_{22} & 2a_{13}a_{23} & a_{12}a_{23}+a_{13}a_{22} & a_{13}a_{21}+a_{11}a_{23} & a_{11}a_{22}+a_{12}a_{21} \end{bmatrix}. \tag{44}$$

Note that we have chosen to let the third rotation angle ψ to be zero, as this is a rotation about the z'-axis and does not alter the growth direction. In the following the primes are omitted. It is also noteworthy that calculations for wurtzite show that all the material parameter tensors as well as the misfit strain contributions do not depend on the angle ϕ (Bykhovski et al., 1993; Chen et al., 2007; Landau & Lifshitz, 1986).

5.2 Static case

In the static case the equations to solve in each layer become

$$\begin{array}{lll} \nabla \cdot \mathbf{T}^{(i)} = 0, & \nabla \cdot D^{(i)} = 0, & \nabla \times \mathbf{E}^{(i)} = 0 \\ \rightarrow \dfrac{\partial T_3^{(i)}}{\partial z} = \dfrac{\partial T_4^{(i)}}{\partial z} = \dfrac{\partial T_5^{(i)}}{\partial z} = 0, & \rightarrow \dfrac{\partial D_z^{(i)}}{\partial z} = 0, & \rightarrow \dfrac{\partial E_x^{(i)}}{\partial z} = \dfrac{\partial E_y^{(i)}}{\partial z} = 0, \end{array} \tag{45}$$

where the superscript i denotes the material, as depicted in Figure 5. Usually one would use homogeneous Dirichlet boundary conditions for the electric field $E_x|_{z=z_l,z_r} = E_y|_{z=z_l,z_r} = 0$, corresponding to the case where the two ends are covered by a perfect conductor. As electric coupling conditions force continuity of the tangential components of $\mathbf{E}$ and these components are constant in each layer we obtain $E_x = E_y = 0$ everywhere. Using the definition of strain we find that in each layer

$$\frac{\partial^2 u_x}{\partial z^2} = \frac{\partial^2 u_y}{\partial z^2} = \frac{\partial^2 u_z}{\partial z^2}, \tag{46}$$

that is, we have linear solutions for the displacement in each layer:

$$u_i = \mathcal{A}_i^{(j)} z' + \mathcal{B}_i^{(j)}. \tag{47}$$

These coefficients are then found by applying continuity of

$$T_3, T_4, T_5, u_x, u_y, u_z, \text{ and } D_z \tag{48}$$

at the material interfaces. At the outer boundaries we will assume free ends

$$T_5 = T_4 = T_3 = 0, D_z = D. \tag{49}$$

The conditions for clamped ends would be $u_x = u_y = u_z = 0$ at the ends. The parameter D is a degree of freedom that in principle corresponds to the application of a voltage across the outer ends (as it changes the electric field and in the static case the electric potential is merely an integration over space). Calculations for a superlattice structure (i.e. a periodic repetition of well and barriers) are exactly the same, with the lattice constants in the well layers adapting to those of the barrier (Poccia et al., 2010).

Calculations for the [111] growth direction of zincblende crystals yields the following analytical expression for the compressional strain in the quantum well (Duggen et al., 2008):

$$S_{zz} = \frac{2\sqrt{3}\frac{e_{x4}^{(2)}}{\epsilon^{(2)}} D + 3\left(c_{11}^{(2)} + 2c_{12}^{(2)}\right) a_{mis}}{4\frac{e_{x4}^{(2)^2}}{\epsilon^{(2)}} + c_{11}^{(2)} + 2c_{12}^{(2)} + 4c_{44}^{(2)}} - a_{mis}. \tag{50}$$

Results for the [111] direction in zincblende quantum wells, with several materials, are given in Table 1. The [111] direction is a rather special case as a compression in the [111] direction yields an electric field in the [111] direction as well and this direction does not couple to the transverse components (i.e. a compression in z-direction does not generate an electric field in x or y directions.) - here zincblende behaves very similar to wurtzite grown along the

[0001] direction. The table also contains a comparison between the fully and the semi-coupled model. The terms S_{semi} and $S_{coupling}$ refer to semi-coupled result and the difference to the fully coupled result, respectively, i.e. $S_{fully-coupled} = S_{semi} + S_{coupling}$.

substrate/QW	S_{semi}	$S_{coupling}$	Deviation	$E'_{z,t}\ [V/\mu\text{m}]$	$E'_{z,e}\ [V/\mu\text{m}]$
GaAs/$In_{0.1}Ga_{0.9}$As	0.34%	−0.002%	0.5%	15.56	17 ± 1[a]
GaAs/$In_{0.2}Ga_{0.8}$As	0.710%	−0.003%	0.4%	28.63	25[b]
AlN/GaN	1.34%	−0.04%	3.1%	271.6	
GaN/$In_{0.3}Ga_{0.7}$N	1.69%	−0.07%	4.4%	355.0	
GaN/InN	7.24%	−0.61%	−9.1%	1441.5	
GaN/AlN	−0.91%	0.04%	−4.7%	−280.3	

[a] Caridi et al. (1990)
[b] J.I.Izpura et al. (1999)

Table 1. Contributions to S'_{zz} in the [111]-grown quantum well layer for different zincblende material compositions with $D = 0$. For GaAs/In_xGa_{1-x}As both $E'_{z,t}$ and $E'_{z,e}$, being the theoretical and the experimental electric field in the QW-layer respectively, are listed for comparison

It can be seen that it does not play a role whether one uses the fully-coupled or the semi coupled approach for the nitrides. Note, however, that the electric field generated by the intrinsic strain in the quantum well layer is quite large and will definitely have an influence on the electrical properties.
The same calculations have been carried out for wurtzite quantum wells (and barriers). For the [0001] growth direction, the analytic result for the compressional strain, which is not coupled to the shear strains in this case, reads (Duggen & Willatzen, 2010; Willatzen et al., 2006)

$$S_{xx} = S_{yy} = -a_{mis}, \tag{51}$$

$$S_{zz}^{(1)} = e_{z3}^{(1)} \frac{D - P_z^{(1)}}{e_{z3}^{(1)^2} + c_{33}^{(1)} \epsilon_{zz}^{(1)}}, \tag{52}$$

$$S_{zz}^{(2)} = \frac{e_{z3}^{(2)}(D - P_z^{(2)}) + 2a_{mis}(e_{z1}^{(2)} e_{z3}^{(2)} + c_{13}^{(2)} \epsilon_{zz}^{(2)})}{e_{z3}^{(2)^2} + c_{33}^{(2)} \epsilon_{zz}^{(2)}}, \tag{53}$$

In principle one can of course find analytic expressions for the general strains as function of the two angles ϕ, θ (for both wurtzite and zincblende). However, these expressions are very cumbersome to comprehend and therefore do not provide additional insight.
Results for the growth direction dependency of a GaN/$Ga_{1-x}Al_xN$/GaN well are shown in Figure 7. For this structure the shear strain is negligible and therefore omitted. For other materials, however the shear strain component is significant and there are significant differences between the fully and semi-coupled approach as seen in Figure 8.
Note that for sufficiently large Al-content, the electric field in the GaAlN well becomes zero at two distinct angles. For the MgZnO structures it shows that there even exist up to three distinct zeros (Duggen & Willatzen, 2010). This is of potential importance as it might lead to increased efficiency for the application of white LEDs (Waltereit et al., 2000).

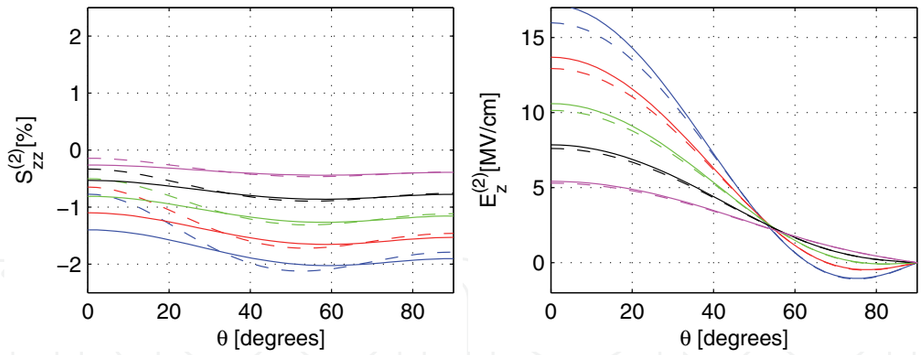

Fig. 7. Compressional strain $S_{zz}^{(2)}$(left) and electric field $E_z(2)$ (right) for $GaN/Ga_{1-x}Al_xN/GaN$ with several x-values and $D = 0\,\mathrm{C/m^2}$. The colors blue, red, green, black, and magenta correspond to $x = 1$, $x = 0.8$, $x = 0.6$, $x = 0.4$, and $x = 0.2$, respectively. Solid (dashed) lines correspond to the semi-coupled (fully-coupled) model. Reprinted with permission from Duggen & Willatzen (2010)

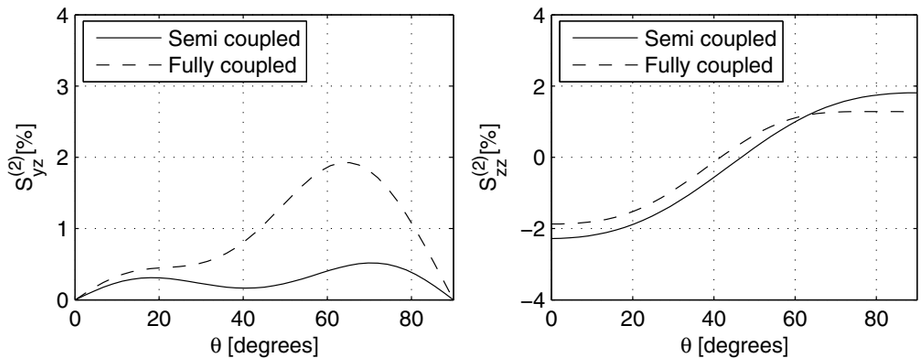

Fig. 8. Shear strain component $S_{yz}^{(2)}$ (left) and compressional strain component S_{zz}^2 (right) in the quantum-well layer of a $Mg_{0.3}Zn_{0.7}O/ZnO/Mg_{0.3}Zn_{0.7}O$ heterostructure for the fully-coupled and semi-coupled models corresponding to $D = 0\,\mathrm{C/m^2}$. Reprinted with permission from Duggen & Willatzen (2010)

5.3 Monofrequency case

Both single quantum wells and for superlattice structures might be subject to an applied alternating electric field, which we will model as application of a monofrequent D-field, i.e. we will assume time harmonic solutions $\propto \exp(i\omega t)$, where $\omega = 2\pi f$ and f is the excitation frequency. Here we will limit us to the zincblende case, but the theory is just as well applicable to wurtzite structures, where one needs to take into account the spontaneous polarization P^{SP} as well.

As the coupling conditions are continuity of $\mathbf{T}$, it is convenient to derive the corresponding differential equation for $\mathbf{T}$. As we assume only z-dependency, Navier's equation becomes three equations:

$$\frac{\partial T_I}{\partial z} = \rho_m \frac{\partial^2 u_i}{\partial z}, \tag{54}$$

where I, i are $3, z$, $4, y$, $5, x$. Furthermore we have that

$$\frac{\partial S_I}{\partial t} = \frac{\partial^2 u_i}{\partial t \partial z}, \tag{55}$$

with the same pairs I, i. Differentiating with respect to z and t, respectively, combining and eliminating $\mathbf{u}$ we obtain

$$\frac{\partial^2 T_I}{\partial z^2} = \rho_m \frac{\partial^2 S_I}{\partial t^2}. \tag{56}$$

Then using the piezoelectric fundamental equation along with the electrostatic approximation (forcing $E_x = E_y = 0$ as in the static case) we obtain the set of three coupled wave equations:

$$\Gamma_{33}\frac{\partial^2 T_3}{\partial z^2} + \Gamma_{34}\frac{\partial^2 T_4}{\partial z^2} + \Gamma_{35}\frac{\partial^2 T_5}{\partial z^2} - \rho_m \frac{\partial T_3}{\partial t^2} = \rho_m \frac{e_{3z}^T}{\epsilon^S}\frac{\partial^2 D_z}{\partial t^2}, \tag{57}$$

$$\Gamma_{43}\frac{\partial^2 T_3}{\partial z^2} + \Gamma_{44}\frac{\partial^2 T_4}{\partial z^2} + \Gamma_{45}\frac{\partial^2 T_5}{\partial z^2} - \rho_m \frac{\partial T_4}{\partial t^2} = \rho_m \frac{e_{4z}^T}{\epsilon^S}\frac{\partial^2 D_z}{\partial t^2}, \tag{58}$$

$$\Gamma_{53}\frac{\partial^2 T_3}{\partial z^2} + \Gamma_{54}\frac{\partial^2 T_4}{\partial z^2} + \Gamma_{55}\frac{\partial^2 T_5}{\partial z^2} - \rho_m \frac{\partial T_5}{\partial t^2} = \rho_m \frac{e_{5z}^T}{\epsilon^S}\frac{\partial^2 D_z}{\partial t^2}, \tag{59}$$

where Γ is the piezoelectrically stiffened elastic tensor. Note that the dispersion relation (which is above equations with $D_z = 0$) is the same as in equation (35) with the weak coupling terms removed as is done with the electrostatic approximation.
The general solution to these wave equations consist of forward and backward propagating waves. The solution in each layer for e.g. the x-polarization reads

$$\begin{aligned} T_5^{(i)} = {} & \mathcal{T}_{5A+}^{(i)} \exp(ik_1 z) + \mathcal{T}_{5A-}^{(i)} \exp(-ik_1 z) + \mathcal{T}_{5B+}^{(i)} \exp(ik_2 z) + \mathcal{T}_{5B-}^{(i)} \exp(-ik_2 z) \\ & + \mathcal{T}_{5C+}^{(i)} \exp(ik_3 z) + \mathcal{T}_{5C-}^{(i)} \exp(-ik_3 z) - \frac{e_{5z}^{(i)T}}{\epsilon^{S(i)}} D_z. \end{aligned} \tag{60}$$

The other polarizations can then be found by solving the dispersion relation for $T_3(k)/T_5(k)$ and $T_4(k)/T_5(k)$. Thus, when the T_5 amplitudes are known, all amplitudes are known. The coupling conditions between the layers are continuity of stress and continuity of particle velocity (corresponding to continuity of particle displacement in the static case), with the particle velocity $\mathbf{v}$ given by

$$\mathbf{v} = \frac{1}{\rho_m \omega}\frac{\partial \mathbf{T}}{\partial z}, \tag{61}$$

where a comment about the dimensionality of $\mathbf{v}$ should be made, since obviously we get elements v_{zx}, v_{zy}, v_{zz}. This is consistent, as the wave has propagation direction z, but three different polarizations x, y, z, i.e. v_5, v_4 describe shear waves while v_3 describes a compressional wave.
The collection of boundary condition equations yields an 18×18 matrix with $\exp(ik_1 z_1)$-like entries. If one would solve for a superlattice consisting of n layers, one would need to solve a $6n \times 6n$ system of equations. As for superlattices this becomes useful when e.g. wanting to

compute a macroscopic speed of sound as one can find resonance frequencies and compare to the expression for resonance frequencies of a homeogeneous material. Note that the intrinsic strain will change the bulk speed of sound of the well material, so one cannot simply use a weighted average of the two sound velocities. Furthermore it is expected that operation at resonance strongly influences the properties of the structure (Willatzen et al., 2006).
The first five resonance frequencies for a zincblende AlN/GaN are shown in Figure 9. It is seen that the transversely dominated resonances (only at [111] the, at this direction degenerate, transverse polarizations are uncoupled from the compressional one) are much lower than the compressionally dominated ones, as one would expect. Thus, when computing resonance frequencies it is important not to compute the ideal [111] direction only, but also take into account the significantly lower frequencies as they might occur due to lattice imperfections (Duggen et al., 2008).

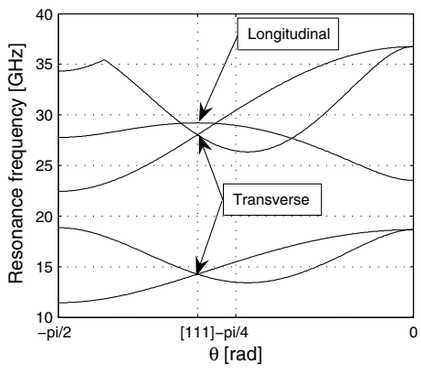

Fig. 9. The first five resonance frequencies for the AlN/GaN structure with $\phi = -\pi/4$. The dimensions of the well-strucure used are 100nm-5nm-100nm. Reprinted with permission from Duggen et al. (2008)

5.4 Cylindrical symmetry of [0001] wurtzite

As we have already noted, the material parameter matrices are invariant under rotation of an angle ϕ around the z-axis. This stipulates investigations of cylindrical structures of wurtzite type. The calculations can, in principle, be done exactly the way described for the quantum well. However, here we consider two degrees of freedom (r, z) which complicates the differential equations and it might not be possible to find analytic solutions anymore. The Voigt notation follows the same standard as for the Cartesian coordinates (including the weight factors) and are

$$rr \to 1,\ \phi\phi \to 2,\ zz \to 3,\ \phi z \to 4,\ rz \to 5,\ r\phi \to 6. \tag{62}$$

The divergence operator becomes

$$\nabla\cdot \to \begin{bmatrix} \frac{\partial}{\partial r}+\frac{1}{r} & -\frac{1}{r} & 0 & 0 & \frac{\partial}{\partial z} & \frac{1}{r}\frac{\partial}{\partial \phi} \\ 0 & \frac{1}{r}\frac{\partial}{\partial \phi} & 0 & \frac{\partial}{\partial z} & 0 & \frac{\partial}{\partial r}+\frac{2}{r} \\ 0 & 0 & \frac{\partial}{\partial z} & \frac{1}{r}\frac{\partial}{\partial \phi} & \frac{\partial}{\partial r}+\frac{1}{r} & 0 \end{bmatrix}, \tag{63}$$

and the material property matrices are transformed in the same manner as for crystal orientation, with

$$\mathbf{a} = \begin{bmatrix} \cos(\phi) & \sin(\phi) & 0 \\ -\sin(\phi) & \cos(\phi) & 0 \\ 0 & 0 & 1 \end{bmatrix}, \tag{64}$$

so since there is cylindrical symmetry, the material parameter matrices remain unchanged. Again using Navier's equation and $\nabla \cdot \mathbf{D} = 0$ one obtains the following linear system of differential equations (with all ϕ-dependencies neglected) (Barettin et al., 2008):

$$L \cdot \begin{bmatrix} u_r \\ u_z \\ V \end{bmatrix} = \begin{bmatrix} -\partial_r \left[(C_{11} + C_{12}) a_{mis} + C_{33} c_{mis} \right] \\ -\partial_z \left[2C_{13} a_{mis} + 2C_{13} c_{mis} \right] \\ -\partial_z p^{SP} \end{bmatrix}, \tag{65}$$

$$\begin{aligned} L = & \begin{bmatrix} \partial_r C_{11} \partial_r + \partial_z C_{ee} \partial_z + 1/r \partial r C_{12} + c_{11} \partial_r 1/r \\ \partial_r C_{44} \partial_z + \partial_z C_{13} \partial_r + \partial_z C_{13}/r + c_{44}/r \partial_z \\ \partial_r e_{15} \partial_z + e_{15}/r \partial_z + \partial_z e_{31} \partial_r + \partial_z e_{15}/r \end{bmatrix} \cdot \begin{bmatrix} 1 & 0 & 0 \end{bmatrix} \\ & + \begin{bmatrix} \partial_r C_{13} \partial z + \partial_z C_{44} \partial r \\ \partial_r C_{44} \partial_r + \partial_z C_{33} \partial_z + C_{44}/r \partial r \\ \partial_r e_{15} \partial_r + e_{15}/r \partial r + \partial_z e_{33} \partial_z \end{bmatrix} \cdot \begin{bmatrix} 0 & 1 & 0 \end{bmatrix} \\ & + \begin{bmatrix} \partial_r e_{31} \partial_z + \partial_z e_{15}/r \partial_r \\ \partial_r e_{33} \partial_z + \partial_z e_{13} \partial_r + e_{15}/r \partial_r \\ -\partial_r \epsilon_{11} \partial_r - \partial_z \epsilon_{33} \partial_z - \epsilon_{11}/r \partial_r \end{bmatrix} \cdot \begin{bmatrix} 0 & 0 & 1 \end{bmatrix}, \end{aligned} \tag{66}$$

where ∂_i is short notation for $\partial/\partial i$ and V is the electric potential (thus $E_z = -\partial_z V$). This system can be solved numerically e.g. by using the Finite Element Method. This has been done for a cylindrical quantum dot structure sketched in Figure 10

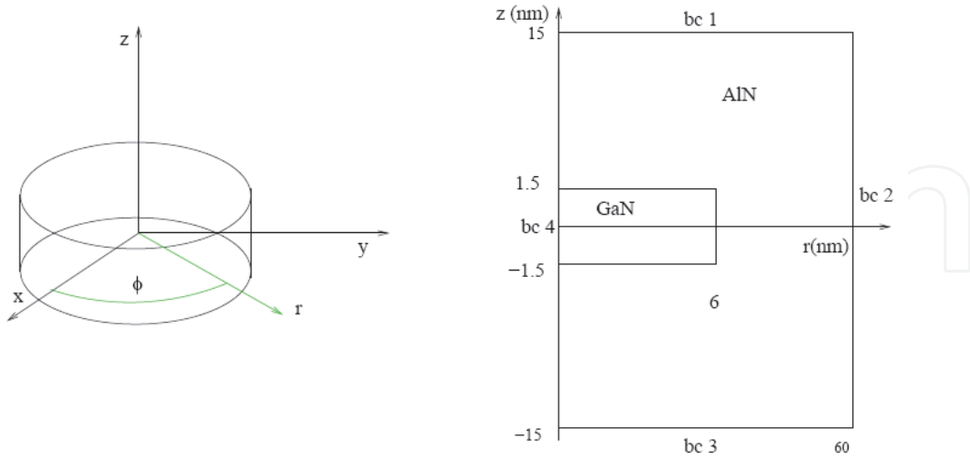

Fig. 10. Geometry of the system under consideration (left) and the two-dimensional equivalent (right). Reprinted with permission from Barettin et al. (2008)

They have found, as can be seen in Figure 11, that the major driving effect for the strain is the lattice mismatch and not the spontaneous polarization.

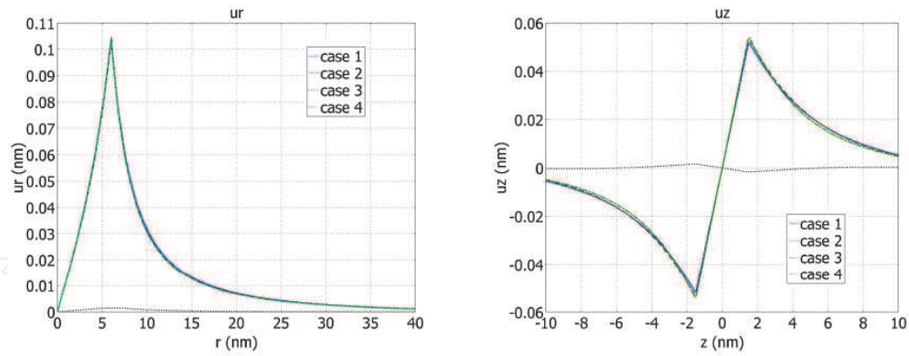

Fig. 11. Displacements u_r at $z = 0$ (left) and u_z at $r = 0$. Four modeling cases are depicted. It suffices to say that only case three does not consider lattice mismatch contributions. Reprinted with permission from Barettin et al. (2008)

Furthermore, using basically the same calculations, Lassen, Barettin, Willatzen & Voon (2008) revealed that calculations in the 3D case can yield a substantially larger discrepancy between semi and fully coupled models, where in the GaN/AlN differences up to 30% were found.

5.5 Other effects

It should be noted that the method described above is by no means secure to be absolutely correct. For example we have disregarded possible free charge densities in order to solve the electromechanical equations self-consistently, without having to solve the Schrödinger equation simultaneously, which would have been necessary otherwise (Voon & Willatzen, 2011). However, it was found by Jogai et al. (2003) that there exists a 2D-electron gas at the interfaces, effectively reducing the generated electric field. Thus the necessity of a fully coupled model is not automatically given, even though calculations as above indicate it.
Also, as already indicated in the piezoelectricity section there might be non-linear effects that are of importance. According to Voon & Willatzen (2011) the effect of non-linear permittivity can be neglected in spite of large electric fields. However, it is not sure whether electrostrictive or second order piezoelectric effects might be of importance. Clearly these questions need further research in order to improve the understanding of electromechanical effects in these structures.

5.6 Alternative: VFF method

As opposed to the above, semi-classical approach there also exist atomistic methods of calculating strains in quantum structures. The are called Valence Force Field (VFF) methods of which Keatings model is the most prominent one (Keating, 1966). Due to limited space we will only present a brief description here, with mainly is taken from Barettin (2009). It should be noted from the start that the piezoelectric effect is not included in this model.
The essence of the model is to impose conditions on the mechanical energy F_s, namely invariance of F_s under rigid rotation and translation as well as symmetries due to the crystal structure. The first condition can be ensured by describing F_s as a function of λ_{klmn}, where

$$\lambda_{klmn} = \left(\vec{u}_{kl} \cdot \vec{u}_{mn} - \vec{U}_{kl} \cdot \vec{U}_{mn} \right) / 2a, \tag{67}$$

where a is the lattice constant, $\vec{U}_{kl} = \vec{X}_k - \vec{X}_l$ with capital $\vec{X}$ denoting nucleus positions in the undeformed crystal and the non-capital $\vec{x}$ denote nucleus positions after deformation. Following assumptions of small deformations and limiting the range of atomic effects to neighboring and second-neighbor terms one arrives at

$$F_s = \frac{1}{2}\sum_{l,l'}\sum_{m,n,m',n'}^{4} B_{mnm'n'}(l-l')\lambda_{mn}(l)\lambda_{m'n'}(l') + O(\lambda^3). \tag{68}$$

where $\lambda_{mn}(l) = \left(\vec{x}_m(l)\cdot\vec{x}_n(l) - \vec{X}_m\cdot\vec{X}_n\right)/2a$ and l denotes the atom cell index (i.e. the atom which neighbors are considered). Within the harmonic approximation one arrives at

$$F_s = \frac{1}{2}\sum_{l}\left[\frac{\alpha}{4a^2}\sum_{i=1}^{4}\left(x_{0i}^2(l) - 3a^2\right)^2 + \frac{\beta}{2a^2}\sum_{i,j>i,1}^{4}\left(x_{0i}(l)\cdot x_{0j}(l) + a^2\right)^2\right], \tag{69}$$

where α, β are empirical elastic parameters. The strain is then found by minimizing the elastic energy F_s, fulfilling boundary conditions as e.g. an imposed dislocation of several atoms at an interface between two materials. The VFF method has also been used to determine ground state configurations of lattice mismatched zincblende structures (Liu et al., 2007) as well as non-binary alloys (Chen et al., 2008).

6. Influence of electromechanical fields on optical properties

Since this book covers optoelectronics, we will also have a brief description of the influence of (piezo)electric fields on the optical properties of a quantum well heterostructure. Instead of using the widely used $k\cdot p$ method with eight bands (Singh, 2003) we will limit ourselves to solve the Schrödinger equation for one band, using the effective mass approximation as also has been done by Lassen, Willatzen, Barettin, Melnik & Voon (2008) for investigating a cylindrical quantum dot.

We need to solve the Schrödinger eigenvalue equation, reading

$$H\Psi = E\Psi, \tag{70}$$

where H is the Hamiltonian and is given by Lassen, Willatzen, Barettin, Melnik & Voon (2008)

$$H = \left(k_z\frac{\hbar^2}{m_e^{||}}k_z + k^{\perp}\frac{\hbar^2}{m_e\ \perp}k^{\perp}\right) + V_{edge} + a_c^{\perp}\epsilon_{zz} + a_c^{\perp}(\epsilon_{xx}+\epsilon_{yy}) - eV, \tag{71}$$

where the m_e denote effective masses, a_c are deformation potentials, e is the fundamental charge, V_{edge} is the band-edge potential. Furthermore, the k-vector is given by $k_j = -i\partial j$ (i being the imaginary unit). Indeed, if one considers a quantum well (i.e. one dimension) there exist analytic solutions to this problem as the Ψ functions can be shown to be linear combinations of Airy functions of first and second kind (Ahn & Chuang, 1986).

The conclusion of the above calculations on a cylindrical quantum dot, performed by Lassen, Willatzen, Barettin, Melnik & Voon (2008) show that the semi-coupled model becomes insufficient when the radius of the quantum dot is comparable or larger than the dot height. In terms of conduction band energy for GaN/AlN the difference between fully and

semi-coupled models is up to 36meV which for large radii is comparable to the conduction band energy itself.

	GaN[a]	AlN[a]	ZnO[b]	MgO[c]
$e_{33}[\mathrm{C/m^2}]$	0.73	0.97	1.32	1.64
$e_{15}[\mathrm{C/m^2}]$	−0.49	−0.57	−0.48	−0.58
$e_{31}[\mathrm{C/m^2}]$	−0.49	−0.57	−0.57	−0.58
$c_{11}^{\mathbf{E}}$[GPa]	390	396	210	222
$c_{12}^{\mathbf{E}}$[GPa]	145	137	121	90
$c_{13}^{\mathbf{E}}$[GPa]	106	108	105	58
$c_{33}^{\mathbf{E}}$[GPa]	398	373	211	109
$c_{44}^{\mathbf{E}}$[GPa]	105	116	42	105
$\epsilon_{xx}^{\mathbf{S}}/\epsilon_0$	9.28	8.67	9.16	9.8[d]
$\epsilon_{zz}^{\mathbf{S}}/\epsilon_0$	10.01	8.57	12.64	9.8[d]
$p^{sp}[\mathrm{C/m^2}]$	−0.029	−0.081	−0.022[c]	−0.068[d]
$a[10^{-10}\mathrm{m}]$	3.189	3.112	3.20[c]	3.45
$c[10^{-10}\mathrm{m}]$	5.185	4.982	5.15[c]	4.14

[a] Fonoberov & Balandin (2003)
[b] Auld (1990)
[c] Gopal & Spaldin (2006)
[d] Park & Ahn (2006)

Table 2. Material parameters. Data for different materials are taken from references indicated in the first row unless otherwise specified. As Fonoberov & Balandin (2003) we assume $e_{15} = e_{31}$ (except for ZnO) and $\epsilon_{xx} = \epsilon_{zz}$ for MgO due to lack of data. We use linear interpolation to obtain parameters for non-binary compounds.

Material	e_{x4}	$c_{11}^E/10^{10}$	$c_{12}^E/10^{10}$	$c_{44}^E/10^{10}$	ϵ^S/ϵ_0	$a/10^{-10}$	ρ_m
$In_{0.1}Ga_{0.9}As$	0.149[a]	11.82	5.55	5.79	13.13[a]	5.6935	5635[b]
GaAs	0.16[a]	12.21	5.66	6.00	12.91[a]	5.6536	5307[b]
GaN	0.50[c]	29.3	15.9	15.5	9.7[c]	4.50	6150[d]
AlN	0.59[c]	30.4	16.0	19.3	9.7[c]	4.38	3245[d]
InN	0.95[f]	18.7	12.5	8.6	14.86[f]	4.98	6810[e]

[a] Caridi et al. (1990)
[b] Auld (1990)
[c] Fonoberov & Balandin (2003)
[d] Average from Willatzen et al. (2006) and Chin et al. (1994)
[e] Chin et al. (1994)
[f] Davydov (2002)

Table 3. Material parameters for incblende structure materials (in SI units). Parameters from Vurgaftman et al. (2001) if not stated otherwise

7. References

Ahn, D. & Chuang, S. L. (1986). Exact calculations of quasibound states of an isolated quantum well with uniform electric field: Quantum-well stark resonance, *Phys. Rev. B* 34(12): 9034–9037.

Auld, B. A. (1990). *Acoustic Fields and Waves in Solids*, Vol. I, Krieger Publishing Company, Malabar, Florida.

Barettin, D. (2009). *Multiphysics effects in quantum-dot structures*, PhD thesis, University of Southern Denmark.

Barettin, D., Lassen, B. & Willatzen, M. (2008). Electromechanical fields in GaN/AlN Wurtzite quantum dots, *Journal of Physics: Conference Series* 107(1): 012001.
URL: *http://stacks.iop.org/1742-6596/107/i=1/a=012001*

Bester, G., Wu, X., Vanderbilt, D. & Zunger, A. (2006). Importance of second-order piezoelectric effects in zinc-blende semiconductors, *Phys. Rev. Lett.* 96(18): 187602.

Bester, G., Zunger, A., Wu, X. & Vanderbilt, D. (2006). Effects of linear and nonlinear piezoelectricity on the electronic properties of InAs/GaAs quantum dots, *Phys. Rev. B* 74(8): 081305.

Bond, W. L. (1943). The mathematics of the physical properties of crystals, *The Bell System Technical Journal* 22(1): 1–72.

Bykhovski, A., Gelmont, B. & Shur, M. (1993). Strain and charge distribution in GaN-AlN-GaN semiconductor-insulator-semiconductor structure for arbitrary growth orientation, *Applied Physics Letters* 63(16): 2243–2245.
URL: *http://link.aip.org/link/?APL/63/2243/1*

Caridi, E., Chang, T., Goossen, K. & Eastman, L. (1990). Direct demonstration of a misfit strain - generated in a [111] growth axis zinc-blende heterostructure, *Applied Physics Letters* 56(7): 659–661.

Chen, C.-N., Chang, S.-H., Hung, M.-L., Chiang, J.-C., Lo, I., Wang, W.-T., Gau, M.-H., Kao, H.-F. & Lee, M.-E. (2007). Optical anisotropy in [hkil]-oriented Wurtzite semiconductor quantum wells, *Journal of Applied Physics* 101(4): 043104.
URL: *http://link.aip.org/link/?JAP/101/043104/1*

Chen, S., Gong, X. G. & Wei, S.-H. (2008). Ground-state structure of coherent lattice-mismatched zinc-blende $a_{1-x}b_xc$ semiconductor alloys ($x = 0.25$ and 0.75), *Phys. Rev. B* 77(7): 073305.

Chin, V. W. L., Tansley, T. L. & Osotchan, T. (1994). Electron mobilities in gallium, indium, and aluminum nitrides, *Journal of Applied Physics* 75(11): 7365–7372.
URL: *http://link.aip.org/link/?JAP/75/7365/1*

Davydov, S. (2002). Evaluation of physical parameters for the group iii nitrates: BN, AlN, GaN, and InN, *Semiconductors* 36: 41–44. 10.1134/1.1434511.
URL: *http://dx.doi.org/10.1134/1.1434511*

Duggen, L. & Willatzen, M. (2010). Crystal orientation effects on Wurtzite quantum well electromechanical fields, *Phys. Rev. B* 82(20): 205303.

Duggen, L., Willatzen, M. & Lassen, B. (2008). Crystal orientation effects on the piezoelectric field of strained zinc-blende quantum-well structures, *Phys. Rev. B* 78(20): 205323.

Fan, W. J., Xia, J. B., Agus, P. A., Tan, S. T., Yu, S. F. & Sun, X. W. (2006). Band parameters and electronic structures of Wurtzite zno and zno/mgzno quantum wells, *Journal of*

Applied Physics 99(1): 013702.
URL: *http://link.aip.org/link/?JAP/99/013702/1*

Fonoberov, V. A. & Balandin, A. A. (2003). Excitonic properties of strained Wurtzite and zinc-blende GaN/$Al_xGa_{1-x}N$ quantum dots, *Journal of Applied Physics* 94(11): 7178–7186.
URL: *http://link.aip.org/link/?JAP/94/7178/1*

Fujita, S., Takagi, T., Tanaka, H. & Fujita, S. (2004). Molecular beam epitaxy of $Mg_xZn_{1-x}O$ layers without wurzite-rocksalt phase mixing from x = 0 to 1 as an effect of ZnO buffer layer, *physica status solidi (b)* 241(3): 599–602.
URL: *http://dx.doi.org/10.1002/pssb.200304153*

Goldstein, H. (1980). *Classical Mechanics*, 2nd edn, Addison Wesley, Cambridge, Massachusetts, USA.

Gopal, P. & Spaldin, N. (2006). Polarization, piezoelectric constants, and elastic constants of ZnO, MgO, and CdO, *Journal of Electronic Materials* 35: 538–542. 10.1007/s11664-006-0096-y.
URL: *http://dx.doi.org/10.1007/s11664-006-0096-y*

Ipatova, I. P., Malyshkin, V. G. & Shchukin, V. A. (1993). On spinodal decomposition in elastically anisotropic epitaxial films of III-V semiconductor alloys, *Journal of Applied Physics* 74(12): 7198–7210.
URL: *http://link.aip.org/link/?JAP/74/7198/1*

J.I.Izpura, Sánchez, J., Sánchez-Rojas, J. & Muñoz, E. (1999). Piezoelectric field determination in strained InGaAs quantum wells grown on [111]b GaAs substrates by differential photocurrent, *Microelectronics Journal* 30: 439–444.

Jogai, B., Albrecht, J. D. & Pan, E. (2003). Effect of electromechanical coupling on the strain in AlGaN/GaN heterojunction field effect transistors, *Journal of Applied Physics* 94(6): 3984–3989.
URL: *http://link.aip.org/link/?JAP/94/3984/1*

Keating, P. N. (1966). Effect of invariance requirements on the elastic strain energy of crystals with application to the diamond structure, *Physical Review* 145(2): 637–645.

Kneissl, M., Treat, D. W., Teepe, M., Miyashita, N. & Johnson, N. M. (2003). Ultraviolet AlGaN multiple-quantum-well laser diodes, *Applied Physics Letters* 82(25): 4441–4443.
URL: *http://link.aip.org/link/?APL/82/4441/1*

Koike, K., Nakashima, I., Hashimoto, K., Sasa, S., Inoue, M. & Yano, M. (2005). Characteristics of a zn[sub 0.7]mg[sub 0.3]o/zno heterostructure field-effect transistor grown on sapphire substrate by molecular-beam epitaxy, *Applied Physics Letters* 87(11): 112106.
URL: *http://link.aip.org/link/?APL/87/112106/1*

Landau, L. & Lifshitz, E. (1975). *Course of Theoretical Physics*, Vol. II: The Classical Theory of Fields, Butterworh Heineman, Oxford, UK.

Landau, L. & Lifshitz, E. (1986). *Course of Theoretical Physics*, Vol. VII: Theory of Elasticity, Butterworh Heineman, Oxford, UK.

Landau, L., Lifshitz, E. M. & Pitaevskii, L. (1984). *Course of Theoretical Physics*, Vol. VIII: Electrodynamics of Continuous Media, Butterworh Heineman, Oxford, UK.

Lassen, B., Barettin, D., Willatzen, M. & Voon, L. L. Y. (2008). Piezoelectric models for semiconductor quantum dots, *Microelectronics Journal* 39(11): 1226 – 1228. Papers CLACSA XIII, Colombia 2007.

Lassen, B., Willatzen, M., Barettin, D., Melnik, R. V. N. & Voon, L. C. L. Y. (2008). Electromechanical effects in electron structure for GaN/AlN quantum dots, *Journal of Physics: Conference Series* 107(1): 012008.
URL: *http://stacks.iop.org/1742-6596/107/i=1/a=012008*

Liu, J. Z., Trimarchi, G. & Zunger, A. (2007). Strain-minimizing tetrahedral networks of semiconductor alloys, *Phys. Rev. Lett.* 99(14): 145501.

Nakamura, S., Mukai, T. & Senoh, M. (1994). Candela-class high-brightness InGaN/AlGaN double-heterostructure blue-light-emitting diodes, *Applied Physics Letters* 64(13): 1687–1689.
URL: *http://link.aip.org/link/?APL/64/1687/1*

Newnham, R. E., Sundar, V., Yimnirun, R., Su, J. & Zhang, Q. M. (1997). Electrostriction: Nonlinear electromechanical coupling in solid dielectrics, *The Journal of Physical Chemistry B* 101(48): 10141–10150.
URL: *http://pubs.acs.org/doi/abs/10.1021/jp971522c*

Park, S.-h. & Ahn, D. (2006). Crystal orientation effects on electronic and optical properties of Wurtzite ZnO/MgZnO quantum well lasers, *Optical and Quantum Electronics* 38: 935–952. 10.1007/s11082-006-9007-y.
URL: *http://dx.doi.org/10.1007/s11082-006-9007-y*

Park, S.-H. & Chuang, S.-L. (1998). Piezoelectric effects on electrical and optical properties of Wurtzite GaN/AlGaN quantum well lasers, *Applied Physics Letters* 72(24): 3103–3105.
URL: *http://link.aip.org/link/?APL/72/3103/1*

Poccia, N., Ricci, A. & Bianconi, A. (2010). Misfit strain in superlattices controlling the electron-lattice interaction via microstrain in active layers, *Advances in Condensed Matter Physics* 2010: 261849.
URL: *http://dx.doi.org/doi:10.1155/2010/261849*

Sasa, S., Ozaki, M., Koike, K., Yano, M. & Inoue, M. (2006). High-performance ZnO/ZnMgO field-effect transistors using a hetero-metal-insulator-semiconductor structure, *Applied Physics Letters* 89(5): 053502.
URL: *http://link.aip.org/link/?APL/89/053502/1*

Singh, J. (2003). *Electronic and Optoelectronic Properties of Semiconductor Structures*, Cambridge University Press, Cambridge, UK.

Voon, L. C. L. Y. & Willatzen, M. (2011). Electromechanical phenomena in semiconductor nanostructures, *Journal of Applied Physics* 109(3): 031101.
URL: *http://link.aip.org/link/?JAP/109/031101/1*

Vurgaftman, I., Meyer, J. & Ram-Mohan, L. (2001). Band parameters for IIIŰV compound semiconductors and their alloys, *Applied Physics Review* 89(11): 5815.

Waltereit, P., Brandt, O., Trampert, A., Grahn, H. T., Menniger, J., Ramsteiner, M., Reiche, M. & Ploog, K. H. (2000). Nitride semiconductors free of electrostatic fields for efficient white light-emitting diodes, *Nature* 406: 865–868.
URL: *http://dx.doi.org/10.1038/35022529*

Willatzen, M. (2001). Ultrasound transducer modeling-general theory and applications to ultrasound reciprocal systems, *IEEE Transactions on Ultrasonics, Ferroelectrics, and Frequency Control* 48(1): 100–112.

Willatzen, M., Lassen, B. & Voon, L. C. L. Y. (2006). Dynamic coupling of piezoelectric effects, spontaneous polarization, and strain in lattice-mismatched semiconductor quantum-well heterostructures, *Journal of Applied Physics* 100(2): 024302.

Yoshida, H., Yamashita, Y., Kuwabara, M. & Kan, H. (2008a). A 342-nm ultraviolet AlGaN multiple-quantum-well laser diode, *Nature Photonics* 1(9): 551–554.
URL: *http://dx.doi.org/10.1038/nphoton.2008.135*

Yoshida, H., Yamashita, Y., Kuwabara, M. & Kan, H. (2008b). Demonstration of an ultraviolet 336 nm AlGaN multiple-quantum-well laser diode, *Applied Physics Letters* 93(24): 241106.
URL: *http://link.aip.org/link/?APL/93/241106/1*

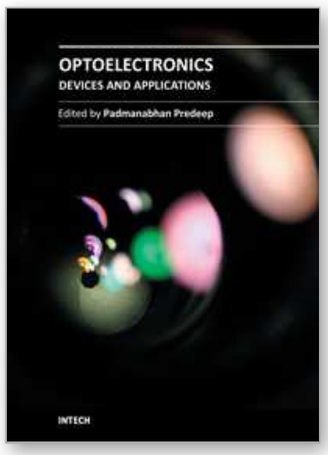

Optoelectronics - Devices and Applications
Edited by Prof. P. Predeep

ISBN 978-953-307-576-1
Hard cover, 630 pages
Publisher InTech
Published online 03, October, 2011
Published in print edition October, 2011

Optoelectronics - Devices and Applications is the second part of an edited anthology on the multifaced areas of optoelectronics by a selected group of authors including promising novices to experts in the field. Photonics and optoelectronics are making an impact multiple times as the semiconductor revolution made on the quality of our life. In telecommunication, entertainment devices, computational techniques, clean energy harvesting, medical instrumentation, materials and device characterization and scores of other areas of R&D the science of optics and electronics get coupled by fine technology advances to make incredibly large strides. The technology of light has advanced to a stage where disciplines sans boundaries are finding it indispensable. New design concepts are fast emerging and being tested and applications developed in an unimaginable pace and speed. The wide spectrum of topics related to optoelectronics and photonics presented here is sure to make this collection of essays extremely useful to students and other stake holders in the field such as researchers and device designers.

INTECH
open science | open minds

InTech Europe
University Campus STeP Ri
Slavka Krautzeka 83/A
51000 Rijeka, Croatia
Phone: +385 (51) 770 447
Fax: +385 (51) 686 166
www.intechopen.com

InTech China
Unit 405, Office Block, Hotel Equatorial Shanghai
No.65, Yan An Road (West), Shanghai, 200040, China
中国上海市延安西路65号上海国际贵都大饭店办公楼405单元
Phone: +86-21-62489820
Fax: +86-21-62489821

IntechOpen